Nat. Hazards Earth Syst. Sci. Discuss., doi:10.5194/nhess-2017-42, 2017
Manuscript under review for journal Nat. Hazards Earth Syst. Sci.
Published: 2 February 2017

Natural Hazards and Earth System Sciences
Discussions

Application of UAV-SfM photogrammetry and aerial LiDAR to a disastrous flood: multitemporal topographic measurement of a newly formed crevasse splay of the Kinu River, central Japan

Atsuto Izumida[1], Shoichiro Uchiyama[1, 2], Toshihiko Sugai[1]

[1]Department of Natural Environmental Studies, the University of Tokyo, Kashiwa, Chiba 277-8563, Japan
[2]National Research Institute for Earth Science and Disaster Prevention, Tsukuba, Ibaraki 305-0006, Japan

Correspondence to: Atsuto Izumida (aizumida@s.nenv.k.u-tokyo.ac.jp)

Abstract. Geomorphic impacts of a disastrous crevasse splay that formed in September 2015 and its post-formation modifications were quantitatively documented by using multitemporal, high-definition digital surface models (DSMs) of an inhabited and cultivated floodplain of the Kinu River, central Japan. The DSMs used were based on pre-flood (resolution, 2 m) and post-flood (resolution, 1 m) aerial light detection and ranging (LiDAR) data from January 2007 and September 2015, respectively, and structure-from-motion (SfM) photogrammetry data (resolution, 3.8 cm) derived from aerial photos taken by an unmanned aerial vehicle (UAV) in December 2015. After elimination of systematic errors among the DSMs, differential DSMs were produced by subtraction and topographic changes on the order of 10^{-1} m were detected. These changes were found to be consistent with previously reported ground survey data. The detected changes included not only topographic changes but also growth of vegetation, vanishing of floodwaters, and restoration and repair works carried out by people. The results suggest that DSMs with different resolutions and acquisition periods acquired by using a combination of UAV-SfM and LiDAR data can be used to quantify, rapidly and in rich detail, sudden topographic changes on floodplains caused by floods. Moreover, they have the great advantage that they can be used to archive such changes that occur in residential areas and urban areas where their preservation potential is low.

1 Introduction

Floods are becoming increasingly serious natural disasters as more and more people move into flood-prone areas along with their assets (Berz et al., 2001; Barredo, 2007; Kundzewicz et al., 2010). Floodplains have long been desirable locations for human habitation owing to their fertile soils and abundant water availability, and many of the world's great cities have been constructed on and have drastically modified the natural environment of floodplains, with the result that flooding in these areas, when it occurs, can be extremely hazardous (Wohl, 2014). When the levee of a river with a sandy bed collapses, crevasse splays (sand splays), that is, discrete lobes or finger-shaped mounds of sandy sediments, and crevasse channels (ephemeral tributaries through which water and sediments are transported onto the floodplain) form, resulting in abrupt, severe topographic changes on the floodplain (Allen, 1965; O'Brien and Wells, 1986; Bristow et al., 1999; Florsheim and Mount, 2002; Day et

Nat. Hazards Earth Syst. Sci. Discuss., doi:10.5194/nhess-2017-42, 2017
Manuscript under review for journal Nat. Hazards Earth Syst. Sci.
Published: 2 February 2017

Natural Hazards and Earth System Sciences
Discussions

al., 2016). Present-day levee breaches along rivers under human control create landforms quite different from and, in some cases, much larger than those created by levee breaches along natural rivers, because of artificial land uses (e.g., human-built structures) along rivers (Nelson and Leclair, 2006) and because the construction of artificial levees raises the potential energy of the flood waters (Gebica and Sokolowski, 2001; Izumida and Sugai, in review). Thus, it is important to determine the volume and area of erosion or deposition that can be expected to occur and how the topographic changes are likely to be distributed on a floodplain during high-magnitude flood events, because these factors directly determine the magnitude and extent of the damages that can be expected to result from a disastrous flood event.

Recently, high-resolution topographic data acquired by innovative remote sensing methods such as aerial and terrestrial light detection and ranging (LiDAR) and structure-from-motion (SfM) photogrammetry has been widely used to evaluate the magnitude of natural hazards (Tarolli, 2014; Gomez and Purdie, 2016). In particular, the combination of SfM with aerial photographs acquired by unmanned aerial vehicles (UAVs) can be very useful in hazardous areas subject to natural disasters such as earthquakes, volcanic eruptions, and landslides, because of the low-cost and mobile operation of UAVs (see Gomez and Purdie, 2016, for a review of each application type).

However, few quantitative descriptions of topography specifically related to a flood disaster on a floodplain are based on high-resolution topographic data obtained by using such methods. Wierzbicki et al. (2013) used post-flood LiDAR data to capture a newly formed crevasse splay of the Vistula River, Poland, but they did not have any pre-flood data for a topographic comparison. The SfM-UAV method has basically not been used to examine floodplain topography in the context of a natural disaster, although Tamminga et al. (2015a) used it in a fluvial setting, applying it to the characterization of the morphology of a gravelly river. Although several studies have performed hydraulic analyses such as mapping floodwaters in urban areas (Feng et al., 2015) and estimation of a basin-scale sediment budget following a large flood (Croke et al., 2013), floodplain topography has attracted less attention from researchers. Reasons may include the low relief and urbanized or agricultural land uses of floodplains (Ninfo et al., 2016), and the low preservation potential of flood-related topography in urban areas (Nelson and Leclair, 2006). Moreover, in many cases, documentation of the topography *before* a flood event is not available, which prevents detailed quantification of flood-caused topographic changes (Tamminga et al., 2015b).

In this study, these difficulties were overcome and UAV and SfM photogrammetry were applied to the case of a disastrous flood that affected an inhabited and cultivated floodplain along the Kinu River, central Japan, in 2015. Three digital surface models (DSMs) of the research area before, 3 days after, and 3 months after the flood were generated by SfM photogrammetry or aerial LiDAR, and the features and post-formation modification of the topography caused by a levee breach were quantitatively documented from the perspective of both natural and artificial changes. In addition, the comparability of topographic data obtained by different acquisition methods and with different resolutions and the use of reference points was examined.

Nat. Hazards Earth Syst. Sci. Discuss., doi:10.5194/nhess-2017-42, 2017
Manuscript under review for journal Nat. Hazards Earth Syst. Sci.
Published: 2 February 2017

Natural Hazards and Earth System Sciences Discussions

2 Study area

The Kinu River, which is 177 km long with a catchment area of 1760 km^2, is one of several large rivers in the Kanto Region, central Japan; it originates in the mountains north of the Kanto Region and joins the Tone River in the central Kanto Plain. Volcanic Neogene and Quaternary age rocks are complexly distributed in the mountains that occupy the upper 60% of its catchment area. The remaining about 35% of the catchment is on the Kanto Plain and consists mainly of the present floodplain of the river and Pleistocene fluvial terraces. Mean annual precipitation is 1600–2100 mm in the mountains, and 1300–1500 mm on the plain.

The area affected by the 2015 flood is located about 50 km northeast from Tokyo (Fig. 1) and about 20 km upstream of the Kinu River's confluence with the Tone River. The Kinu River in this area has low sinuosity and a sandy bed with a gradient of about 1/2500, and it flows southward. The Kinu River and the Kokai River, another tributary of the Tone River, flow along the western and eastern margin, respectively, of a floodplain, and each river is surrounded by alluvial ridges 1–2 m higher than flood basin, which occupies the center of the floodplain. The floodplain itself is 4–8 km wide, and it is bordered on both the east and west by fluvial terraces (Fig. 1). The largest alluvial ridges, which are 1.5–2 km wide, are those to the east of the Kinu River in Joso City. Older crevasse channels dissect the wide alluvial ridges by 1 m in depth, suggesting that the Kinu River has flooded repeatedly in this region (Sadakata, 1971).

In fact, repeated flooding of the Kinu and Kokai rivers around the study area during the past several hundred years is documented in the historical record, although how each flood affected the topography of the floodplain is unclear. Two floods occurred recently along the Kokai River, in 1981 and 1986. During the 1981 flood, a crevasse splay was formed at a point 4 km upstream of its confluence with the Tone River, where the Kokai River intersected an abandoned channel, creating a sandy mound more than 60 cm thick and a crevasse channel (breach scouring) with a length of 200 m and a depth of 2 m (Iseya et al., 1982).

3 The 2015 flood of the Kinu River

A levee breach of the Kinu River at Joso City, Ibaraki Prefecture, which occurred on 10 September 2015, was caused by a record heavy rain during 7–11 September, particularly during 9–10 September, driven by Typhoon Etau and the extratropical cyclone it became. The total rainfall during the period of heavy rain exceeded 600 mm along the upper reaches of the Kinu River, and 200–300 mm along the central to lower reaches (JMA, 2015). At a gauge station located 10 km upstream from the breached levee, the peak water level, which was more than 6 m higher than the ordinary water level, was recorded on 10 September. The artificial levee on the left bank of the Kinu River collapsed on the same day and resulted in the formation of a crevasse splay on the alluvial ridge (Figs. 2 and 3).

The levee breach and other outflows from the Kinu River inundated an area of 40 km^2 on the floodplain between the Kinu and Kokai rivers; this area is equivalent to one-third of the area of Joso City. The flood water reached a depth of more than 2.5 m in the flood basin and the inundation depth of the alluvial ridges was generally 1 m or less near the breached levee, while

Nat. Hazards Earth Syst. Sci. Discuss., doi:10.5194/nhess-2017-42, 2017
Manuscript under review for journal Nat. Hazards Earth Syst. Sci.
Published: 2 February 2017

Natural Hazards and Earth System Sciences Discussions

the depth increased to 1.5 m or more in the south of the floodplain and decreased to 0.5 m or less, or none far from the breached levee (Nagumo et al., 2016). It took 10 days of pumping to remove the flood water from the levee-protected floodplain; 6000 of the 65,000 inhabitants of Joso City had to be evacuated, and the flood damaged, destroyed, or inundated 5000 buildings, in addition to causing severe interruptions of public utilities and the transportation system (Joso City, 2016). The breached levee had been temporarily repaired by two weeks after the flood, thus preventing additional flooding of the Kinu River (KRDB, 2015).

Because of the rarity of levee-breaching floods on inhabited floodplains in modern Japan, the 2015 flood of the Kinu River attracted a great deal of attention and prompted many investigations, including remote surveys of the damaged floodplain. One of the topographic data sets that we used in this study was a DSM constructed by using aerial LiDAR data acquired 3 days after the flood.

4 Method

4.1 Data acquisition and DSM generation

4.1.1 LiDAR data

Two sets of LiDAR measurement data, acquired on 15 January 2007, before the flood, and on 13 September 2015, 3 days after the flood, were used in this study (Table 1). Land use in the study area is mainly agricultural (cultivated land), except for the area next to the levee, and it was largely bare of vegetation in winter when the first data set was acquired. Moreover, when the second data set was acquired immediately after the flood, the crops had been almost flattened by the flood waters. Thus, the data are considered to be fairly accurate without any adjustment for surface objects such as vegetation and buildings. These data sets included georeferenced orthophotos.

LiDAR data before the flood were provided by the Kanto Regional Development Bureau, Land, Infrastructure and Transportation Ministry of Japan. The measurement point density was 1.2 points m^{-1} in the east–west direction, and 1.3 points m^{-1} in the north–south direction (i.e., 0.64 points m^{-2}). The pixel size of the DSM was set to 2 m so that each pixel contained two measurement points on average. We generated a DSM from these data by using the 3D Analyst extension of ESRI ArcGIS 10.2.2 Desktop software. The Create TIN tool was first used to construct a triangular irregular network (TIN) of the data, and then the TIN was converted to a DSM by using a TIN to Raster tool.

LiDAR data were acquired soon after the flood by Aero Asahi Corp. (AAC). The measurement point density was 0.43 points m^{-1} (i.e., 5.4 points m^{-2}). The DSM of these data was generated by AAC by the TIN method, and the pixel size was set to 1 m.

During the LiDAR measurement, the position of the aircraft was determined by GNSS equipment, and the inclination of the aircraft (roll, pitch, and yaw) was logged by an internal measurement unit. The on-board position information was corrected by using ground reference stations with known coordinates, established by a static GNSS survey.

Nat. Hazards Earth Syst. Sci. Discuss., doi:10.5194/nhess-2017-42, 2017
Manuscript under review for journal Nat. Hazards Earth Syst. Sci.
Published: 2 February 2017

Natural Hazards and Earth System Sciences Discussions

4.1.2 UAV–SfM data

On 26 December 2015, we conducted a flight campaign with a UAV (DJI F550 six-rotor multicopter equipped with an APM 2.6 flight controller) over the alluvial ridge where significant topographic changes had been caused by the flood to obtain high-resolution measurements and to characterize the post-formation modifications of the crevasse splay. The flight was automatically piloted by an APM Mission Planner ground station; the UAV's height was maintained at 150 m above ground level and its speed was maintained 10 m s^{-1} while the photographs were being acquired. The UAV was equipped with a Ricoh GR digital camera (focal length, 18.3 mm; resolution, 16.2 megapixels) and weighed about 2.4 kg altogether. Six flights, each 15 min long, were conducted over 2 h on the morning of 26 December, and 1433 photos were taken at 2-s intervals. However, these included many unusable photos that were taken when the UAV was not flying along the planned path, for example, while it was ascending or descending (5 m s^{-1} and 2.5 m s^{-1}). Finally, of the 1433 photos, 597 photos with an 80% overlap both across and along the UAV paths were analyzed with the SfM technique to generate a DSM.

We used Agisoft Photoscan Pro 1.2.1 software for automatic camera calibration and the SfM analysis. The DSM was georeferenced by 15 ground control points (GCPs) obtained by a real-time kinematic (RTK) GNSS using a Trimble Geo 7X instrument and Zephyr Model 2 antenna with a horizontal and vertical accuracy of 5 cm. Flat places with low relief such as a paved road were selected for the GCP locations. The ground resolution of the resulting DSM was 3.84 cm, and it covered an area of about 0.793 km^2. The root mean square error (RMSE) of the DSM with 15 GCPs was 2.37 cm in the east-west direction, 2.14 cm in the north-west direction, and 1.58 cm in the elevation, and 3.56 cm overall.

4.2 Evaluation of the horizontal accuracy of DSMs

To validate that an object was represented at the same location on all DSMs, each of which had been georeferenced independently, the gradient of each pixel was calculated for the three DSMs, and the edges of the same houses and other buildings were identified independently on the three slope rasters (Fig. 4). In Fig. 4, high slope areas are white, so the boundaries between vertical structures such as buildings and walls or trees and the ground appear as white belts. The lines indicating building edges and walls on the December 2015 gradient map are located in the center of the high slope areas of the DSMs for the other two dates. This relationship was confirmed to be the same at several locations (not shown). Because the high slope areas are wide when the resolution of the original DSM is low, it is the resolution of the DSM, rather than its horizontal accuracy, that matters when evaluating topographic changes by raster comparison.

4.3 Calculation of differential rasters

Raster subtraction of DSMs for successive dates allows the topographic changes occurring between the two dates to be evaluated. Comparison of the DSMs for the first two dates (before and soon after the flood) shows the direct impact of the flood on the topography of the floodplain, and comparison of the DSMs for the second two dates shows post-formation modification of the crevasse splay.

Nat. Hazards Earth Syst. Sci. Discuss., doi:10.5194/nhess-2017-42, 2017
Manuscript under review for journal Nat. Hazards Earth Syst. Sci.
Published: 2 February 2017

Natural Hazards and Earth System Sciences Discussions

Before the differential rasters could be calculated, it was necessary to evaluate the systematic errors between pairs of DSMs. The systematic error between each comparison set was determined by selecting more than 10 points at locations that were stable between the two dates and assigning the mean elevation difference at each of those points to the systematic error (Table 2). The selected comparison points were located on flat areas where little change was observed between the two dates and which were wider than the pixel sizes of the DSMs. In the process of eliminating the systematic errors, the resolution of the SfM-derived DSM was reduced to 1/10 by computing the mean value of the original pixels with the Aggregate tool of the ArcGIS software because its original resolution was much higher than that of the other two DSMs.

The comparison results showed that elevations on the January 2007 DSM were higher than those on the September 2015 DSM by 37.9 cm ± 4.5 cm (mean ± standard deviation), and those on the September 2015 DSM were lower than those on the December 2015 DSM by 20.6 cm ± 1.8 cm. Thus, topographic changes on the order of 10^{-1} m could be represented by these DSMs. The absolute height of the topography was set to the December 2015 DSM values, the GCPs of which had been accurately measured with RTK GNSS. The DSMs were processed with the ArcGIS Raster Calculator tool to obtain two differential rasters (Fig. 5). The resolution and pixel distribution of each differential raster were the same as those of the DSM with the higher resolution of each pair.

5 Results and discussion

5.1 Overview of the topography of the alluvial ridge and crevasse splay on each date

The DSMs and aerial orthophotos of the research area provide three snapshots of the study area, from before (January 2007), shortly after (September 2015), and 3 months after (December 2015) the flood (Fig. 2). The research area was on the southern part of an alluvial ridge along the Kinu River, the width of which was about 1.5 km (Fig. 1). Within the research area, the elevation of the ridge was high along the channel, especially near the breached levee, although the ground level there might have been raised for construction. The artificial levee was about 2 m higher than the top of the alluvial ridge. The alluvial ridge was divided by a shallow valley oriented north–south along the eastern margin of the study area, which Sadakata (1971) suggested was a past crevasse channel. In 2007, an agricultural canal ran along the valley, and a network of smaller canals covered the research area. The part of the alluvial ridge in the study area (Fig. 2a) was mainly used for cultivating agricultural crops; most of the area was not covered by pavement or buildings except close to the levee. It has been estimated, therefore, that the effect of human modifications to the landscape on the crevasse splay formation was quite small (Izumida and Sugai, in review).

The levee breach caused changes to the topography up to 300–500 m away from the levee; sand splays composed of well-sorted medium sand were deposited, a crevasse channel was eroded, and structures and other artificial features near the breached levee were damaged or destroyed (Fig. 2b, 3; Izumida and Sugai, in review). The crevasse channel was elongated to the east and then curved southward following the shallow valley. Breach scouring, that is, deep, distinguishable ditches, were created in the proximal part of the crevasse channel (Fig. 3c), but they and some other erosional areas were still submerged in

Nat. Hazards Earth Syst. Sci. Discuss., doi:10.5194/nhess-2017-42, 2017
Manuscript under review for journal Nat. Hazards Earth Syst. Sci.
Published: 2 February 2017

Natural Hazards and Earth System Sciences Discussions

September 2015 (Fig. 3a), so their elevations on the DSM were interpolated from the elevations along the margins of the pools. Buildings, cars, the prefectural road along the levee, and other artificial features were washed away by the flood and some of them came to rest within the crevasse channel (Fig. 3d). In the channel behind these obstacles, relatively small, elongated sandy mounds up to 150 m long were deposited. Sand splays were deposited to the north and south of the obstacles, with clear terminations on their downstream sides (Fig. 3b). The southern splays, 150–200 m long and 100 m wide, were larger than the northern ones.

Three months after the flood (December 2015), the crevasse channel was no longer submerged, and the areas of sand deposition appeared lighter in color than other, more muddy areas (Fig. 2c). Other than natural changes, some restoration and repair works by humans were apparent. The breached levee had already been repaired temporarily, the scouring along prefectural road had been partly filled and leveled, and the road had been reopened. Modification of the immediate post-flood topography was less in distal areas, although some changes are visible in the DSM and orthophoto: for example, crops had grown or been cut in the agricultural lands, and sediments trapped in the canal had been removed along with the obstacles within the crevasse channel. Numerous wheel tracks on the ground indicate that many vehicles (Fig. 6b) had been driven across the study area after the flood, even where marked modification of the topography was not observed.

5.2 Comparison of DSMs between January 2007 and September 2015

Figure 5a shows the differential raster between the DSM before (January 2007) and that 3 days after (September 2015) the flood. Areas where the differences between the two DSMs are less than 0.1 m after removal of the systematic error are transparent, showing the September 2015 orthophoto used as the background. Areas of the crevasse channel that were submerged in September 2015 show topographic changes related to the water surface, not the bottom of the crevasse channel, in the differential raster. Near the levee, the erosional depth exceeded 1 m, decreasing to the east. In the shallow valley formed by the past crevasse channel, however, the topography showed a little aggradation, despite the apparent continuity of the surface seen in the orthophotos (Fig. 2); the aggradation is probably attributable to the presence of crops before the flood and the submergence of the land surface in September 2015. The thickness of the sand splays was estimated to be up to 60 cm in the north and 80 cm in the south, except where small sandy mounds had aggraded behind obstacles on the sand splays. At the downstream end of the splays, the splay height was 30–50 cm relative to the adjacent ground, consistent with the field survey results (Izumida and Sugai, in review). Small sandy mounds behind the obstacles with heights of 20 cm or more are recognizable in the differential raster.

In addition to the obvious topographic changes, some more subtle changes were detected. For example, aggradation of 10 cm or more was widely observed beyond both the north and south sand splays, and in some locations, the deposition exceeded 50 cm. However, because the systematic error between the DSMs was removed by using the elevation of the paved road, the differential raster represents not only changes caused by the 2015 flood but also changes in the status of the agricultural lands, such as the presence of crops and the soil built up over the course of more than eight years. Careful evaluation of such changes is needed for a more detailed discussion of flood-related changes.

Nat. Hazards Earth Syst. Sci. Discuss., doi:10.5194/nhess-2017-42, 2017
Manuscript under review for journal Nat. Hazards Earth Syst. Sci.
Published: 2 February 2017

Natural Hazards and Earth System Sciences Discussions

5.3 Comparison between DSMs of September 2015 and December 2015

The differential raster of the DSMs between 3 days after (September 2015) and 3 months after (December 2015) the flood is shown in Fig. 5b. Significant topographic changes can be observed where restoration works exceeded those completed immediately after the flood. The most remarkable change is the temporary repair of the breached levee, which was raised in height by up to 5.5 m (>1 m in the figure). The area to the east of the repaired prefectural road seemed mostly flat in the December 2015 DSM and orthophoto, but in fact the amount of fill varied between 10 and 60 cm compared with the original scour topography. In contrast, up to 100 cm of flood deposits were removed to level the ground in the depositional area near the levee. Several buried canals were restored by excavation, and the sand was heaped on both sides of the canals. In the case of the large canal on the east side of the research area, however, the removed sand had been transported elsewhere by December 2015. Other than in those areas, the crevasse splay was left mostly undisturbed, so its features were deformed only by natural phenomena occurring during the 3 months after the flood.

The first natural modification was the emergence of the submerged areas of the crevasse channel (Fig. 6a). The values of the differential raster along the formerly submerged crevasse channel indicate the depth of the pool, because the September 2015 DSM shows mostly the elevation of the water surface in that area. Thus, by using the two differential rasters, the water depth in the crevasse channel 3 days after the flood can be estimated as well as the total amount of erosion of the alluvial ridge. They show that the water depth was 20–60 cm, and erosion of up to 150 cm, with higher values near the levee, was caused by the flood. In the restored areas along the breached levee, however, the true erosional depth of the scouring, certainly the most significant within the study area, could not be determined from the DSMs because the scouring was filled in before the UAV flight was conducted. This is an example of the difficulties faced in the investigation of disasters in developed regions.

In the areas that had been covered with muddy sediments, such as beyond the sand splay in the northern part of the study area (Fig. 6b), shrubs with heights up to 30 cm grew up after the flood. In natural floodplains, crevasse splay development promotes the formation of new colonies of vegetation (Florsheim and Mount, 2002; Cahoon et al., 2011); thus, such new growth might be an important environmental component of the floodplain if there had been no human changes to the crevasse splay. Because each shrub is less than 1 m high, and they are distributed separately, they would be difficult to observe by LiDAR alone because of the limited resolution of the measured points. Usage of the UAV-SfM method to generate DSMs was therefore more suitable for documenting the relatively subtle changes in this case.

As in previous reports of the topography of crevasse splays (O'Brien and Wells, 1986; Bristow et al., 1999), steep slopes formed at the downstream edges of the crevasse splays in the research area. Three months after their formation, however, the eastern edges of the southern splays had aggraded 10–20 cm, and the western edge of one splay had been lowered by 10 cm (Fig. 6c, d), indicating that sand composing the splay had moved eastward. This direction coincides with the direction of the seasonal wind in winter in Japan (Table 3). Available wind data from after the flood show that on 63 of 100 days the dominant wind direction was between northerly and westerly, which could account for the low gradient of the splay edges. The dry wintertime climate of Japan might also help the sand to be easily moved by the wind.

Nat. Hazards Earth Syst. Sci. Discuss., doi:10.5194/nhess-2017-42, 2017
Manuscript under review for journal Nat. Hazards Earth Syst. Sci.
Published: 2 February 2017

Natural Hazards and Earth System Sciences Discussions

5.4 Recording of landforms with low preservation potential by combined usage of UAV-SfM and LiDAR

In this study, the systematic error between DSMs was assumed to be merely the average of the elevation differences at several selected points. In fact, almost all parts of the road, which were assumed to be stable throughout, were shown to experience small elevation changes (<10 cm) in both comparison pairs (Fig. 5). This result suggests that even the simple elimination method used in this study can effectively detect differences on the order of 10^{-1} m in topographic data acquired by different methods and at different times.

The resolution of the LiDAR-derived DSM is much lower than the resolution of that produced by the UAV-SfM method, but it was possible to compare the topography at finer scale than the LiDAR data by fitting the pixels of the differential raster to the UAV-derived DSM, because actual topography at the earlier time was simpler than that at the later time. In particular, where the topographic relief is small and vegetation is sparse, as in the study area, even relatively low resolution topographic data is adequate for describing and archiving the effects of a disaster on the topography through comparisons with high-resolution data obtained after the event.

Of course, pre-flood topographic data are necessary to quantify the degree of erosion and deposition. In Japan, open-access LiDAR data with a resolution of 5 m covering the whole country except for some remote areas is available from the Geospatial Information Authority of Japan (Sato et al., 2010) and can be used for comparison with data obtained after disasters. For example, Saito et al. (2016) utilized a combination of UAV-SfM topographic data obtained after a heavy rainfall in the mountains of southeastern Japan and available pre-hazard LiDAR data to estimate sediment yields of landslides. This study and that of Saito et al. (2016) both took advantage of the availability of UAVs, which because of their low cost and flexible operation, can be effectively used to obtain topographic measurements for use in combination with past LiDAR data to determine topographic differences related to sudden events. Furthermore, UAVs can easily be used to obtain additional topographic data on successive dates to produce '4D' topographic models, that is, 3D models showing the evolution of the measurement objectives over time (Gomez and Purdie, 2016). This study achieved this at a very primitive level by using DSMs obtained at three different times to estimate inundation depth and shrub growth. A similar multitemporal analysis of topography would be possible in other areas in Japan and anywhere else in the world where extensive topographic measurements have been made; thus, this method is expected to become applicable to more and more regions. The accumulation of knowledge about the nature of hazardous earth surface processes is expected to help us to mitigate the damage suffered by people and human society from future disasters.

In the context of disaster management, high-resolution photos and videos taken by UAVs can help in the development of strategies to take in the event of emergencies (Ezequiel et al., 2014; Erdelj and Natalizio, 2016). Another UAV 'eye', namely, topographic data obtained by SfM photogrammetry, would also be informative, particularly if acquired immediately after the occurrence of a disaster. Applications suggested by the results of this study include volume estimation of flood deposits that need to be removed and, conversely, the amount of materials necessary for the construction of embankments or for land filling. Evaluation of these possibilities, however, exceeds the scope of this paper.

Nat. Hazards Earth Syst. Sci. Discuss., doi:10.5194/nhess-2017-42, 2017
Manuscript under review for journal Nat. Hazards Earth Syst. Sci.
Published: 2 February 2017

Natural Hazards and Earth System Sciences Discussions

6 Conclusions

In this study, multitemporal topographic data acquired by UAV-SfM photogrammetry and LiDAR, with a resolution on the order of 10^{-2} and 10^{0} m, respectively, were successfully used to quantify topographic changes on a floodplain caused by the 2015 flood of the Kinu River, including the formation of a crevasse splay and its post-formation modification by both natural and artificial causes. All three topographic data sets used in this study were surface models, but in the most of the research area, they represented the ground elevation because there were few buildings and little vegetation except for agricultural crops. The horizontal accuracy of the DSMs estimated from the positions of building edges showed that the difference in resolution of the DSMs determined the accuracy of the comparisons made by raster calculations. Elevation differences on the order of 10^{-1} m were detectable between pairs of DSMs after the removal of the systematic error. However, care is needed to account for environmental changes due the difference in the time of acquisition, such as vegetation growth and ground modification by humans.

Multitemporal measurement of the topography allowed the post-formation modifications of the crevasse splay to be quantified. Through the use of surface models, not only changes to the topography itself but also to vegetation, the inundating water, and artificial modifications for restoration and repair could be quantified. The relatively low resolution of the LiDAR-derived DSM limited detailed quantification of the topography, but subtle changes on a horizontal scale smaller than the pixel size of the LiDAR-derived DSM were detectable in the comparison with a DSM acquired later by the UAV-SfM method because the topography in the earlier DSM was relatively simple.

Low-cost and speedy data acquisition (2 h in the field to cover 0.793 km^2 in this study) by UAV can be effectively used, particularly when used in combination with LiDAR data obtained beforehand, to capture topography related to natural disasters with low preservation potential because they are in inhabited regions, where the affected topography is likely to be restored soon after the disaster. Because river floods and the consequent formation of crevasse splays occur in floodplains around the world, the accumulation of similar studies will promote our understanding of the splay formation process and enable damages caused by such flooding to be mitigated. To achieve this goal, however, the preparation and maintenance of an extensive LiDAR database is needed to make possible quantification of topographic changes caused by floods and other disasters by UAV-SfM photogrammetry.

7 Data availability

The aerial photos taken from the UAV and SfM-processed DSM are not open to the public for further analysis by the authors. The post-flood LiDAR and orthophotos are provided to the authors with special permission of Aero Asahi Corp. The pre-flood LiDAR data and orthophotos are available with permission from Kanto Regional Development Bureau, Ministry of Land, Infrastructure, Transport and Tourism. The climate data in Joso City are freely available from Japan Meteorological Agency (http://www.jma.go.jp/jma/menu/menureport.html).

Author contributions A. Izumida undertook the processing and the interpretation of the data and the preparation of the manuscript with contributions from all co-authors. S. Uchiyama undertook the data acquisition with the UAV and the SfM processing. T. Sugai designed the research and gave the final approval of the article.

Competing interests. The authors declare that they have no conflict of interest.

Acknowledgement. We gratefully thank Hiroshi Kobayashi of Aero Asahi Corporation for providing the processed DSM derived from the post-flood LiDAR data and the orthophotos acquired in September 2015. This study was financially supported by JSPS KAKENHI Grant Number JP26282078.

References

Allen, J. R. L.: a Review of the Origin and Characteristics of Recent Alluvial Sediments, Sedimentology, 5(2), 89–191, doi:10.1111/j.1365-3091.1965.tb01561.x, 1965.

Barredo, J. I.: Major flood disasters in Europe: 1950-2005, Nat. Hazards, 42(1), 125–148, doi:10.1007/s11069-006-9065-2, 2007.

Berz, G., Kron, W., Loster, T., Rauch, E., Schimetschek, J., Schmieder, J., Siebert, A., Smolka, A. and Wirtz, A.: World map of natural hazards - a global view of the distribution and intensity of significant exposures, Nat. Hazards, 23(2–3), 443–465, doi:10.1023/A:1011193724026, 2001.

Bristow, C. S., Skelly, R. L. and Ethridge, F. G.: Crevasse splays from the rapidly aggrading, sand-bed, braided Niobrara River, Nebraska: Effect of base-level rise, Sedimentology, 46(6), 1029–1047, doi:10.1046/j.1365-3091.1999.00263.x, 1999.

Cahoon, D. R., White, D. A. and Lynch, J. C.: Sediment infilling and wetland formation dynamics in an active crevasse splay of the Mississippi River delta, Geomorphology, 131(3–4), 57–68, doi:10.1016/j.geomorph.2010.12.002, 2011.

Croke, J., Todd, P., Thompson, C., Watson, F., Denham, R. and Khanal, G.: The use of multi temporal LiDAR to assess basin-scale erosion and deposition following the catastrophic January 2011 Lockyer flood, SE Queensland, Australia, Geomorphology, 184, 111–126, doi:10.1016/j.geomorph.2012.11.023, 2013.

Day, J. W., Cable, J. E., Lane, R. R. and Kemp, G. P.: Sediment deposition at the caernarvon crevasse during the great Mississippi flood of 1927: Implications for coastal restoration, Water (Switzerland), 8(2), doi:10.3390/w8020038, 2016.

Erdelj, M. and Natalizio, E.: UAV-Assisted Disaster Management: Applications and Open Issues, 9th Int. Work. Wirel. Sensor, Actuator Robot Networks (WiSARN 2016), 2016.

Ezequiel, C. A. F., Cua, M., Libatique, N. C., Tangonan, G. L., Alampay, R., Labuguen, R. T., Favila, C. M., Honrado, J. L. E., Canos, V., Devaney, C., Loreto, A. B., Bacusmo, J. and Palma, B.: UAV aerial imaging applications for post-disaster assessment, environmental management and infrastructure development, 2014 Int. Conf. Unmanned Aircr. Syst., 274–283, doi:10.1109/ICUAS.2014.6842266, 2014.

Feng, Q., Liu, J. and Gong, J.: Urban flood mapping based on unmanned aerial vehicle remote sensing and random forest classifier-A case of yuyao, China, Water (Switzerland), 7(4), 1437–1455, doi:10.3390/w7041437, 2015.

Florsheim, J. L. and Mount, J. F.: Restoration of floodplain topography by sand-splay complex formation in response to intentional levee breaches, Lower Cosumnes River, California, Geomorphology, 44(1–2), 67–94, doi:10.1016/S0169-555X(01)00146-5, 2002.

Gebica, P. and Sokolowski, T.: Sedimentological interpretation of crevasse splays formed during 1997 flood in the Vistula River Valley (South Poland), Ann. Soc. Geol. Pol., 71, 53–62, 2001.

Gomez, C. and Purdie, H.: UAV- based Photogrammetry and Geocomputing for Hazards and Disaster Risk Monitoring – A Review, Geoenvironmental Disasters, 3(1), 23, doi:10.1186/s40677-016-0060-y, 2016.

Iseya, F., Ikeda, H. and Mikami, Y.: Topographic changes at levee breached area of the Kokai River in August, 1981, Bull. Environ. Res. Ctr., Univ. of Tsukuba, 6, 117, 1982 (in Japanese).

Izumida, A. and Sugai, T.: Formation of a crevasse splay at an artificial levee breached during the 2015 flood of the Kinu River, Central Japan: implications for fluvial geomorphology, Geomorphology, in review.

Japan Meteorological Agency (JMA): Natural phenomenon report for disasters 1, [online] Available from: http://www.jma.go.jp/jma/kishou/books/saigaiji/saigaiji_2015/saigaiji_201501.pdf (Accessed 13 January 2017), 2015 (in Japanese).

Joso City: Inspection report on actions for the 2015 flood of the Kinu River in Joso City, [online] Available from: http://www.city.joso.lg.jp/ikkrwebBrowse/material/files/group/6/kensyou_houkokusyo.pdf (Accessed 23 January 2017), 2016 (in Japanese).

Kanto Regional Development Bureau (KRDB): Actions for the 2015 Kanto and Tohoku Heavy Rain (18th report). [online] Available from: http://www.ktr.mlit.go.jp/ktr_content/content/000633310.pdf (Accessed 11 January 2017), 2015 (in Japanese).

Kundzewicz, Z. W., Hirabayashi, Y. and Kanae, S.: River Floods in the Changing Climate-Observations and Projections, Water Resour. Manag., 24(11), 2633–2646, doi:10.1007/s11269-009-9571-6, 2010.

Nagumo, N., Ohara, M., Kuribayashi, D., Sawano, H. and Kinu, R.: The 2015 Flood Impact due to the Overflow and Dike Breach of Kinu River in Joso City , Japan, J. Disaster Res., 11(6), 1112–1127, doi:10.20965/jdr.2016.p1112, 2016.

Nelson, S. a. and Leclair, S. F.: Katrina's unique splay deposits in a New Orleans neighborhood, GSA Today, 16(9), 4, doi:10.1130/GSAT01609A.1, 2006.

Ninfo, A., Mozzi, P. and Abbà, T.: Integration of LiDAR and cropmark remote sensing for the study of fluvial and anthropogenic landforms in the Brenta-Bacchiglione alluvial plain (NE Italy), Geomorphology, 260, 64–78, doi:10.1016/j.geomorph.2015.11.006, 2016.

O'Brien, P. E. and Wells, a. T.: A small, alluvial crevasse splay, J. Sediment. Res., 56(6), 876–879, doi:10.1306/212F8A71-2B24-11D7-8648000102C1865D, 1986.

Sadakata, N.: Formation of the Lower Kinu River Floodplain, Geographical Sciences (Chiri Kagaku), 18, 13–22, 1971 (in Japanese with English abstract).

Saito, H., Uchiyama, S., Obanawa, H. and Hayakawa, Y. S.: Sediment yields triggered by heavy rainfall in July 2012 at Aso Volcano: application of high-definition topography data using unmanned aerial vehicles and structure-from-motion multi-view stereo photogrammetry, Geographical Review of Japan Series A, 89(6), 347–359, 2016 (in Japanese with English abstract).

Sato, H., Iwahashi, J., Koarai, M., Kamiya, I. and Komuro, K.: Preparation of high-resolution digital elevation models by the Geospatial Information Authority of Japan and their applications to geographic information analysis, Transactions, Transactions, Japanese Geomorphological Union, 31(4), 359–382, 2010 (in Japanese with English abstract).

Tamminga, A., Hugenholtz, C., Eaton, B. and Lapointe, M.: Hyperspatial remote sensing of channel reach morphology and hydraulic fish habitat using an unmanned aerial vehicle (UAV): a first assessment in the context of river research and management. River Research and Applications, River Res. Appl., 31(3), 379–391, doi:10.1002/rra.2743, 2015a.

Tamminga, A. D., Eaton, B. C. and Hugenholtz, C. H.: UAS-based remote sensing of fluvial change following an extreme flood event, Earth Surf. Process. Landforms, 40(11), 1464–1476, doi:10.1002/esp.3728, 2015b.

Tarolli, P.: High-resolution topography for understanding Earth surface processes: Opportunities and challenges, Geomorphology, 216, 295–312, doi:10.1016/j.geomorph.2014.03.008, 2014.

Wierzbicki, G., Ostrowski, P., Mazgajski, M. and Bujakowski, F.: Using VHR multispectral remote sensing and LIDAR data to determine the geomorphological effects of overbank flow on a floodplain (the Vistula River, Poland), Geomorphology, 183, 73–81, doi:10.1016/j.geomorph.2012.06.020, 2013.

Wohl, E.: Rivers in the Landscape: Science and Management, Wiley-Blackwell, Chichester, UK., 2014.

Nat. Hazards Earth Syst. Sci. Discuss., doi:10.5194/nhess-2017-42, 2017
Manuscript under review for journal Nat. Hazards Earth Syst. Sci.
Published: 2 February 2017

Natural Hazards and Earth System Sciences
Discussions

Table 1. Timeline of data acquisition in relation to the levee breach and information on the DSMs used in this study.

Date	Data acquisition method	Resolution of DSM
15 January 2007	LiDAR	2.0 m
10 September 2015	Levee breach at Joso City	
13 September 2015	LiDAR	1.0 m
26 December 2015	UAV	3.84 cm

Nat. Hazards Earth Syst. Sci. Discuss., doi:10.5194/nhess-2017-42, 2017
Manuscript under review for journal Nat. Hazards Earth Syst. Sci.
Published: 2 February 2017

Natural Hazards and Earth System Sciences
Discussions

Table 2: Points used to compare each pair of DSMs

Comparison pair	Number of points compared	Maximum elevation difference between points (cm)	Minimum elevation difference between points (cm)	Mean elevation difference between points (cm)	Standard deviation of the difference between points (cm)
Jan 2007–Sep 2015	11	45.9	28.8	37.9	4.5
Sep 2015–Dec 2015	15	23.1	15.7	20.6	1.8

Nat. Hazards Earth Syst. Sci. Discuss., doi:10.5194/nhess-2017-42, 2017
Manuscript under review for journal Nat. Hazards Earth Syst. Sci.
Published: 2 February 2017

Natural Hazards and Earth System Sciences
Discussions

Table 3: Dominant wind directions from 18 September to 26 December 2015 at Joso Observatory of JMA. Data are from the JMA (http://www.jma.go.jp/jma/menu/menureport.html).

Dominant wind direction	Number of days	Mean wind velocity (m s^{-1})
E	7	1.46
ENE	2	1.75
NE	0	0
NNE	1	1.10
N	20	1.69
NNW	23	1.53
NW	10	1.09
WNW	6	2.73
W	4	1.73
WSW	3	1.00
SW	2	1.30
SSW	1	1.00
S	2	1.65
SSE	3	1.27
SE	5	0.94
ESE	11	1.67

Nat. Hazards Earth Syst. Sci. Discuss., doi:10.5194/nhess-2017-42, 2017
Manuscript under review for journal Nat. Hazards Earth Syst. Sci.
Published: 2 February 2017

Natural Hazards and Earth System Sciences
Discussions

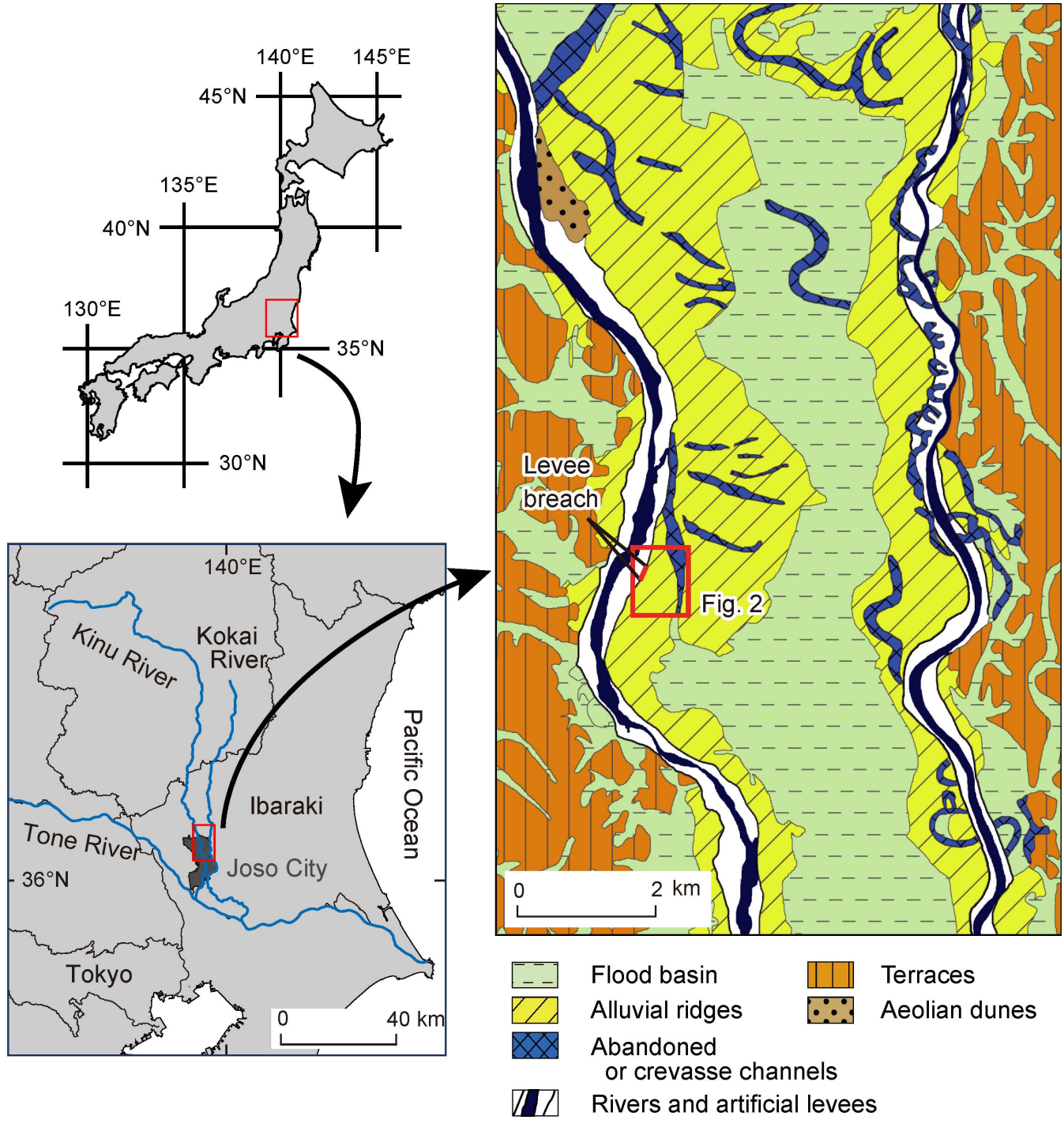

Figure 1: Location map of Joso City and the Kinu River, and geomorphic map showing the location of the levee breeched during the 2015 flood. Modified from Izumida and Sugai (in review).

Nat. Hazards Earth Syst. Sci. Discuss., doi:10.5194/nhess-2017-42, 2017
Manuscript under review for journal Nat. Hazards Earth Syst. Sci.
Published: 2 February 2017

Natural Hazards and Earth System Sciences
Discussions

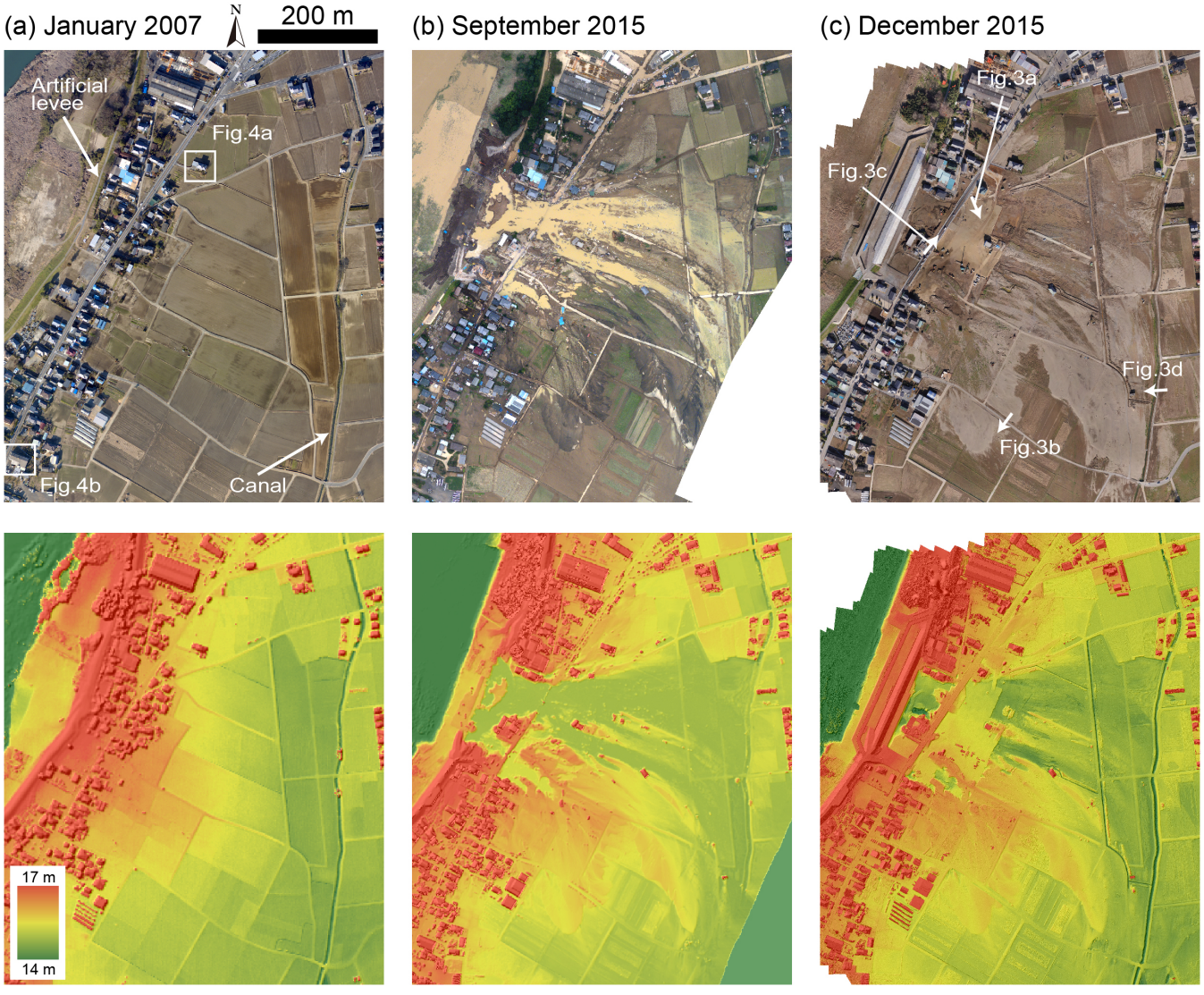

Figure 2: The three DSMs and orthophotos used in this study. See the text for the information about the acquisition of each data set. Elevations are relative to mean sea level in Tokyo Bay. Note the research area does not correspond to the extent of these DSMs.

5

Nat. Hazards Earth Syst. Sci. Discuss., doi:10.5194/nhess-2017-42, 2017
Manuscript under review for journal Nat. Hazards Earth Syst. Sci.
Published: 2 February 2017

Natural Hazards and Earth System Sciences
Discussions

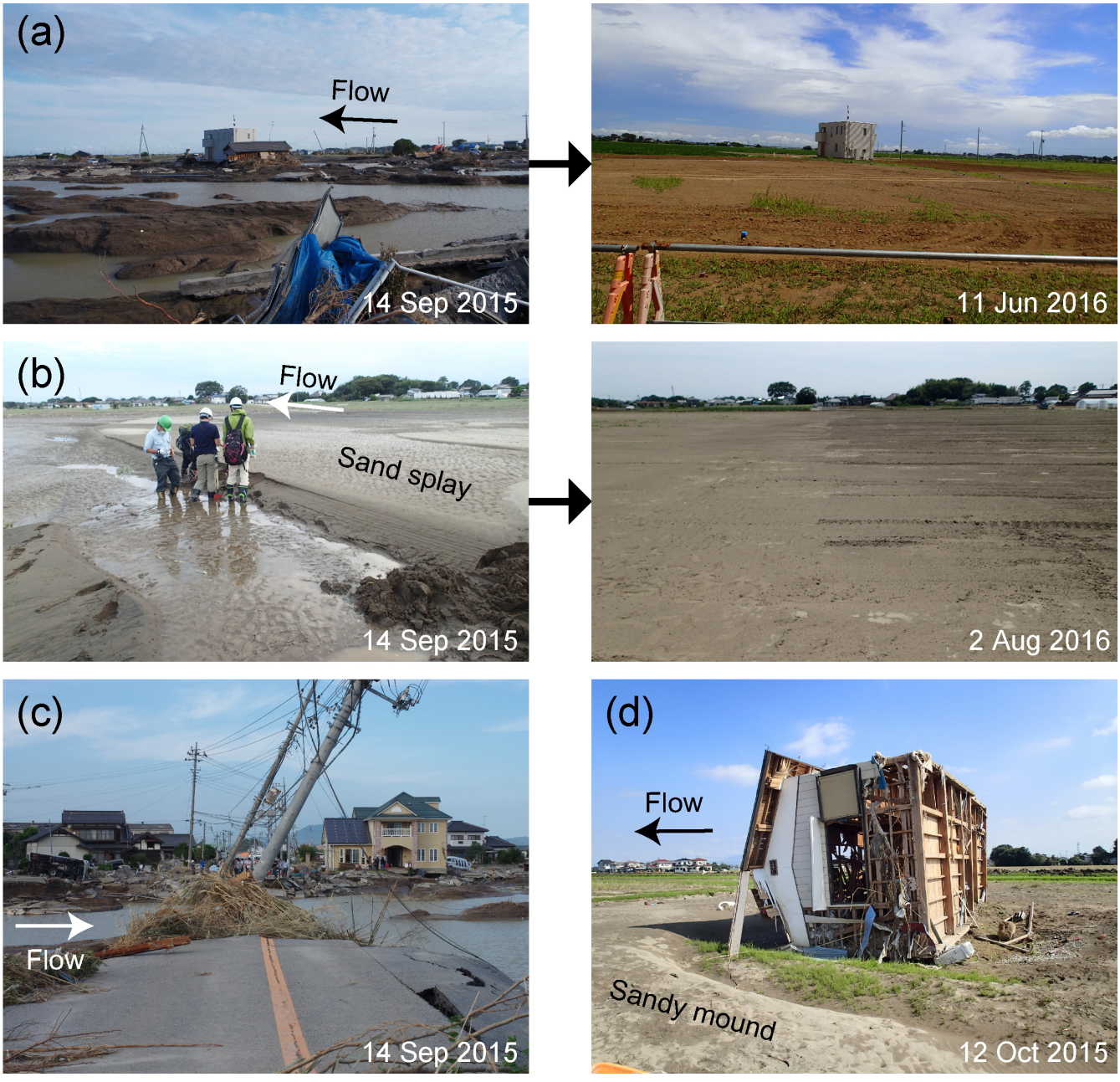

Figure 3: Photos of the study area. (a) Crevasse channel (breach scouring) near the levee (left) and the same place after the scour was filled in (right). Note the building still standing after the flood in the center of the photos. (b) Sand splay in the southern part of the study area (left) and the same place after the sand had been removed (right). (c) Damaged prefectural road beside the breached levee. (d) Overturned and transported house. Note the sandy mound in the downstream direction from the house. See Fig. 2c for the photo locations. Photos were taken by A. Izumida and T. Sugai.

Nat. Hazards Earth Syst. Sci. Discuss., doi:10.5194/nhess-2017-42, 2017
Manuscript under review for journal Nat. Hazards Earth Syst. Sci.
Published: 2 February 2017

Natural Hazards and Earth System Sciences
Discussions

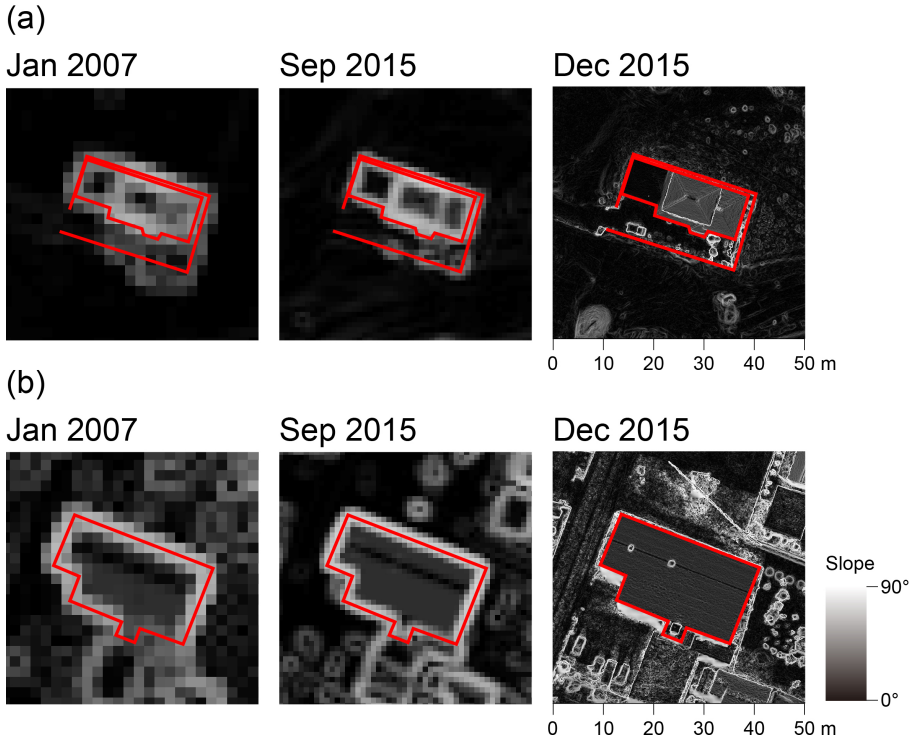

Figure 4: Gradient maps showing two buildings used to evaluate the horizontal accuracy of the DSMs. The cell sizes are the same as in the originals. Red lines indicate the edges of the buildings or walls on the December 2015 map. Note that these lines are within high slope areas on the maps for the other two dates. See Fig. 2a for the locations.

Nat. Hazards Earth Syst. Sci. Discuss., doi:10.5194/nhess-2017-42, 2017
Manuscript under review for journal Nat. Hazards Earth Syst. Sci.
Published: 2 February 2017

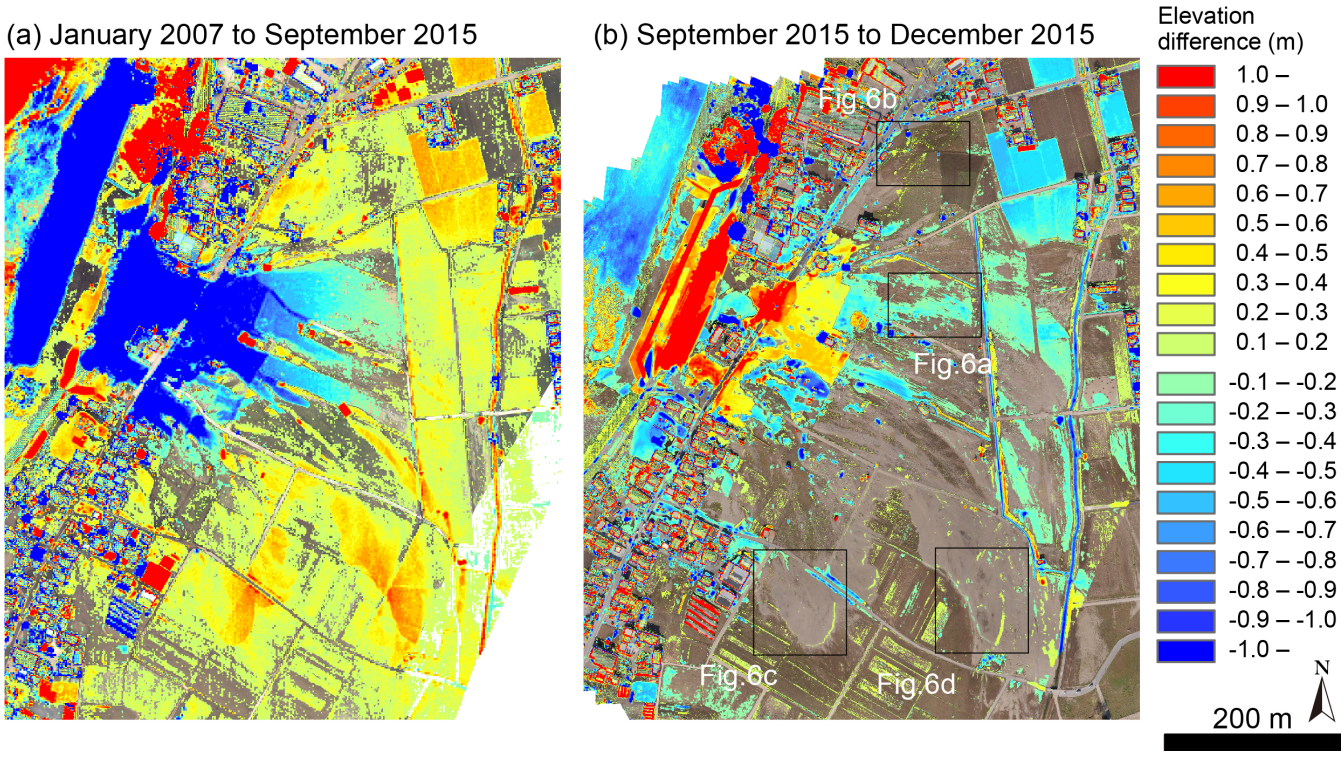

Figure 5: Differential rasters indicating the elevation differences between two successive snapshots after the removal of the systematic error. (a) The January 2007 DSM subtracted from the September 2015 DSM. Note that erosion near the breached levee was more than 1 m. (b) The September 2015 DSM subtracted from the December 2015 DSM. Enlarged views of several locations are shown in Fig. 6.

Nat. Hazards Earth Syst. Sci. Discuss., doi:10.5194/nhess-2017-42, 2017
Manuscript under review for journal Nat. Hazards Earth Syst. Sci.
Published: 2 February 2017

Natural Hazards and Earth System Sciences
Discussions

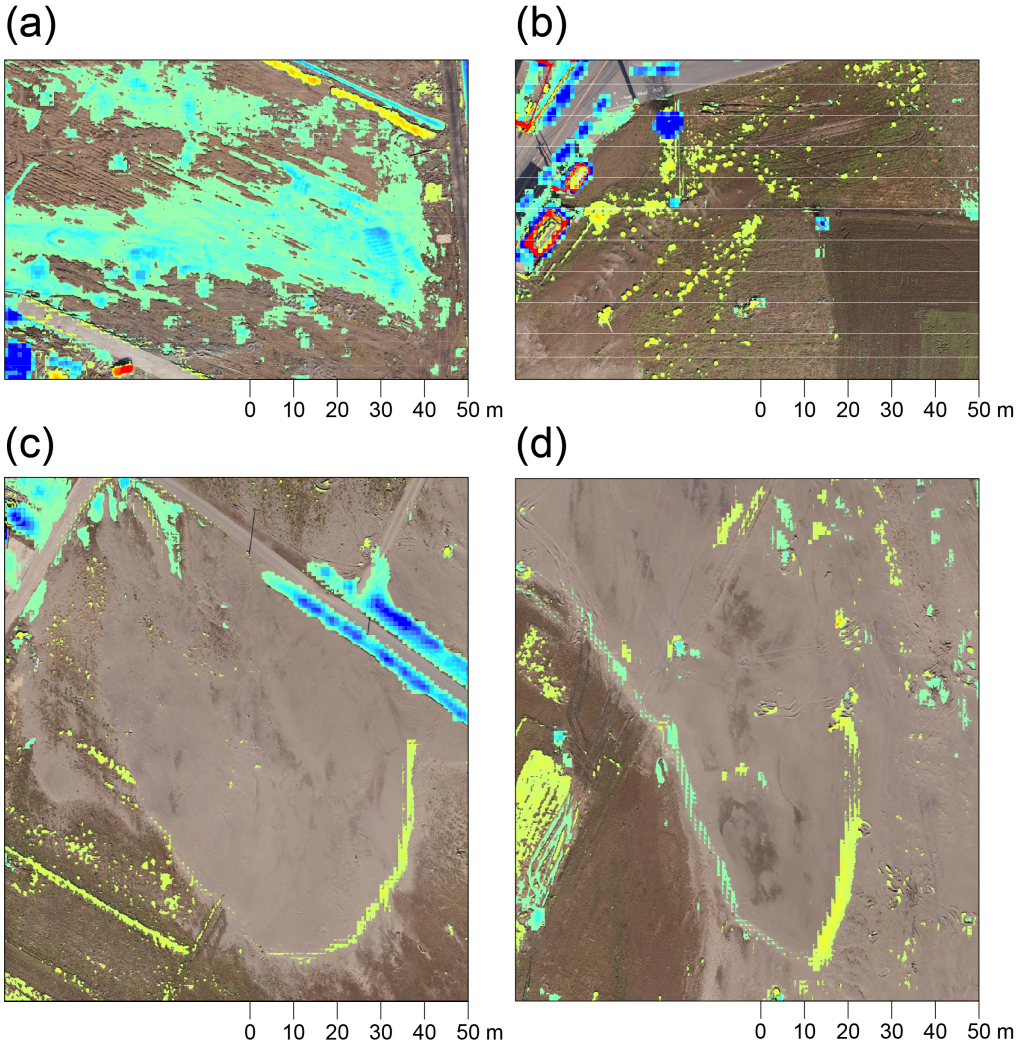

Figure 6: Enlarged views of areas of the differential raster between the September and December 2015 DSMs (Fig. 5b) showing where the topography of the crevasse splay was changed during the research period by specific processes. (a) The bottom of the crevasse channel after evaporation of the flood water. (b) Some newly grown shrubs. (c) and (d) Sand remobilized by the seasonal northwesterly winter winds and moved to the edges of sand splays.